ACS central science

Outlook

Cite This: ACS Cent. Sci. 2018, 4, 324−336

Recent Development of Inorganic Nanoparticles for Biomedical Imaging

Dokyoon Kim,[†] Jonghoon Kim,[†,‡] Yong Il Park,[*,§] Nohyun Lee,[*,∥] and Taeghwan Hyeon[*,†,‡]

[†]Center for Nanoparticle Research, Institute for Basic Science (IBS), Seoul 08826, Republic of Korea

[‡]School of Chemical and Biological Engineering, and Institute of Chemical Processes, Seoul National University, Seoul 08826, Republic of Korea

[§]School of Chemical Engineering, Chonnam National University, Gwangju 61186, Republic of Korea

[∥]School of Advanced Materials Engineering, Kookmin University, Seoul 02707, Republic of Korea

ABSTRACT: Inorganic nanoparticle-based biomedical imaging probes have been studied extensively as a potential alternative to conventional molecular imaging probes. Not only can they provide better imaging performance but they can also offer greater versatility of multimodal, stimuli-responsive, and targeted imaging. However, inorganic nanoparticle-based probes are still far from practical use in clinics due to safety concerns and less-optimized efficiency. In this context, it would be valuable to look over the underlying issues. This outlook highlights the recent advances in the development of inorganic nanoparticle-based probes for MRI, CT, and anti-Stokes shift-based optical imaging. Various issues and possibilities regarding the construction of imaging probes are discussed, and future research directions are suggested.

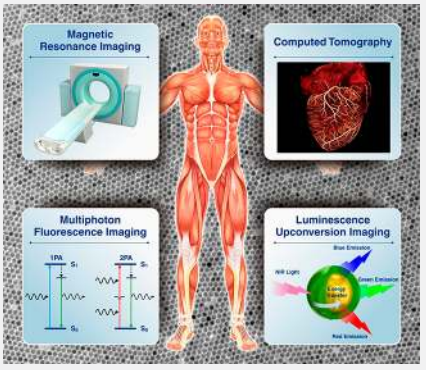

INTRODUCTION

Bioimaging refers to the visualization of biological structures and processes. A variety of techniques with their own advantages have been developed for that purpose to meet the needs in various clinical and laboratory settings.[1−4] In many cases, imaging probes that can label target molecules or organs are used to provide enhanced visibility and to enable the acquisition of more detailed structural and functional information.[5−7] Consequently, the use of imaging probes is becoming indispensable for biological research and disease diagnosis.

Recent advances in the development of imaging probes have led to the bioimaging at subcellular or molecular level.[8−10] That said, the majority of the imaging probes currently used in clinics are organic molecules or metal−organic compounds,[11−13] whose utility is limited because of their intrinsic physical and physiological properties. To list a few examples, fluorescent dyes used for optical imaging suffer from photobleaching,[14] and magnetic resonance imaging (MRI) contrast agents made of Gd^{3+}-chelates exhibit weak contrast effect due to their low magnetic moment.[15] These small molecule-based probes also have a short circulation time *in vivo*, resulting in poor targeting efficiency and insufficient imaging enhancement.[16]

Nanotechnology has facilitated the development of unprecedented imaging probes with outstanding performance.[17−19] Inorganic nanoparticles are one of the most widely studied materials in this regard due to their unique physical and chemical properties that originate from their nanoscale dimensions.[20] Various nanoparticle probes for bioimaging were developed using their magnetic, X-ray attenuation, and optical properties (Figure 1). For example, magnetic nanoparticles (e.g., superparamagnetic iron oxide nanoparticles) have been applied as strong T_2 MRI contrast agents, showing much improved detection sensitivity over conventional Gd^{3+}-based MRI contrast agents.[21−23] Nanoparticles of high-Z elements (e.g., gold,[24,25] bismuth,[26−28] and tantalum[29,30]) have been studied for enhanced computed tomography (CT) contrast agents owing to their high X-ray attenuation. The better optical and chemical stability of quantum dots (QDs) and their relatively easily tunable emission wavelength compared with those of fluorescent dyes enable the use of QDs as robust fluorescent tags in optical imaging.[31−33] Despite these advantages, inorganic nanoparticle-based imaging probes still have many drawbacks that prevent their extensive use in clinical settings, which include magnetic susceptibility artifacts of T_2 MRI contrast agents,[34] photoinduced tissue damage from ultraviolet (UV) excitation source for QDs,[35] and potential toxicity of heavy metal-containing nanoparticles.[36,37] As a result, very few nanoparticle probes are approved for clinical use.

Many efforts have been made in recent years to address the limitations of typical inorganic nanoparticle imaging probes. To overcome the intrinsic limitations of T_2 MRI, extremely small iron oxide nanoparticles were utilized as T_1 MRI contrast agents.[38,39] Shallow tissue penetration depth of UV excitation could be circumvented by using near-infrared (NIR) light for

Received: December 4, 2017
Published: January 23, 2018

DOI: 10.1021/acscentsci.7b00574
ACS Cent. Sci. 2018, 4, 324−336

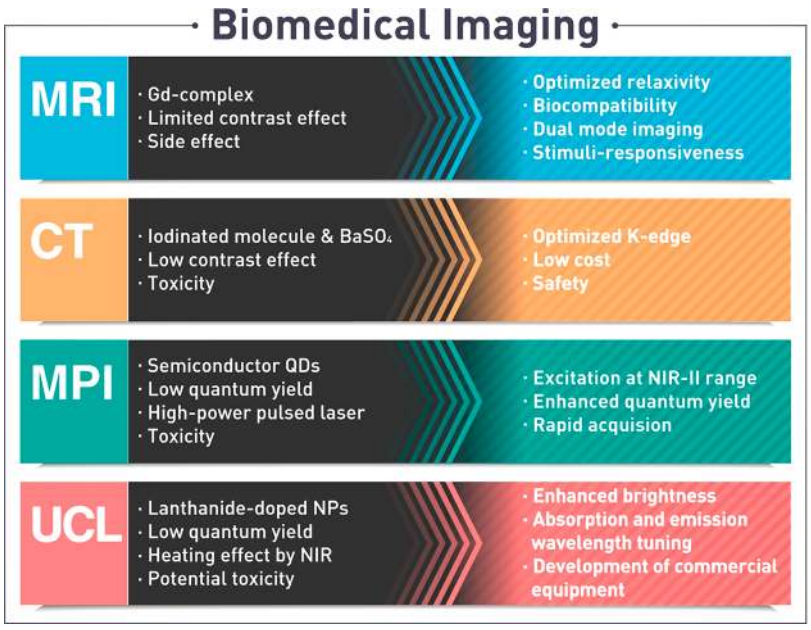

Figure 1. Current status of inorganic nanoparticle-based bioimaging and future direction.

> Nanotechnology has facilitated the development of unprecedented imaging probes with outstanding performance.

the excitation of nanoparticle probes.[40−43] Moreover, several nanoparticle surface modification methods have been developed to provide enhanced biocompatibility and functionalities such as stimuli-responsiveness, targeted imaging, and therapy.[44]

Here, we focus on the recent progress in inorganic nanoparticle probes for MRI, CT, and anti-Stokes shift-based optical imaging, of which the characteristics are summarized in Table 1. We discuss various issues that need to be considered when developing nanoparticle probes. Finally, we propose future research directions for the next generation imaging probes.

MRI CONTRAST AGENTS

MRI is a noninvasive medical imaging technique based on the principle of nuclear magnetic resonance (NMR).[45] In a strong magnetic field, hydrogen nuclei absorb resonant radiofrequency pulses, and subsequently the excited nuclei return to the initial state by emitting the absorbed radio frequency energy. MRI contrast is generated by the different relaxation characteristics of the hydrogen atoms in tissues that are affected by the presence of nearby magnetic materials. For example, paramagnetic materials enhance the longitudinal relaxation processes (also called T_1 relaxation processes), producing brighter MR signal, while superparamagnetic and ferromagnetic materials accelerate the transverse relaxation processes (also called T_2 relaxation processes), resulting in hypointense MR signal. Using these properties, complexes of paramagnetic gadolinium ions (Gd^{3+}) and superparamagnetic iron oxide nanoparticles (SPIONs) have been used as T_1 and T_2 contrast agents, respectively.[46] Recently, though, most nanoparticle-based MRI contrast agents have been withdrawn from the market, leaving Gd(III) complexes to dominate the current market for the MRI contrast agents.[47]

This situation brings up a question: is it still worth pursuing nanoparticle-based MRI contrast agents? To deal with this question, it is necessary to consider various factors including safety, efficacy, and market shares. First-generation magnetic nanoparticle-based T_2 MRI contrast agents such as Feridex and Resovist were used to detect liver lesions, and second-generation agents such as Combidex were developed for the diagnosis of lymph metastases.[34] They were withdrawn from the market not for safety concerns, but rather due to their small market shares: T_1 contrast agents are preferred in clinics due to bright MR images, and more importantly, Gd(III)-based T_1 contrast agents are able to cover most organs including the liver.[48] Furthermore, the contrast effects of the early generation magnetic nanoparticle-based contrast agents were not sufficiently strong owing to their small core size and low crystallinity.[49]

Newly developed magnetic nanoparticles have a strong chance to compete with the Gd(III)-based contrast agents.[17]

Table 1. Characteristics of Various Nanoparticle-Based Imaging Modalities

imaging modality	imaging probe	spatial resolution	molecular sensitivity	maximum penetration depth
magnetic resonance imaging (MRI)	para-/superpara-/ferromagnetic nanoparticles (Gd, Fe, Mn, etc.)	∼100 μm	μM−mM	no limit
computed tomography (CT)	nanoparticles of high-Z elements (Ba, I, Au, Ta, etc.)	∼100 μm	∼1 mM	no limit
anti-Stokes shift-based optical imaging	doped quantum dots, upconverting nanoparticles	<1 μm	<1 μM	<1 mm

DOI: 10.1021/acscentsci.7b00574
ACS Cent. Sci. 2018, 4, 324−336

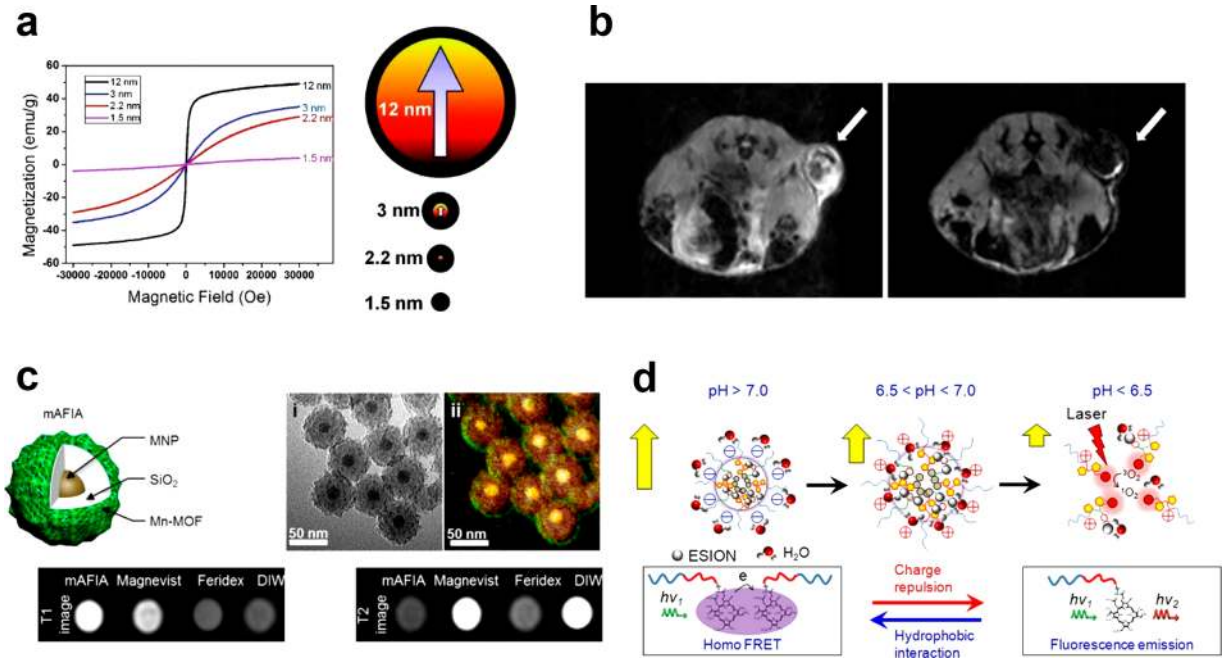

Figure 2. (a) Field-dependent magnetization ($M-H$) curves at 300 K for iron oxide nanoparticles of various sizes (left). Description of the spin canting effect in the iron oxide nanoparticles of various sizes (right). (b) *In vivo* MR images of the xenografted tumor before (left) and after (right) intravenous administration of FIONs. (c) Artifact filtering imaging agent (mAFIA) that comprises a combination of paramagnetic Gd-MOF and superparamagnetic nanoparticles for T_1-T_2 dual-mode MRI. (d) Tumor pH-responsive magnetic nanogrenades composed of self-assembled extremely small-sized iron oxide nanoparticles and pH-sensitive ligands. Reprinted with permission from refs 21, 38, 67, and 74. Copyright 2011, 2012, and 2014 American Chemical Society.

First, while a serious side effect of Gd(III) complexes, such as nephrogenic systemic fibrosis, is an issue of major concern,[50] iron oxides are generally regarded as benign and biologically tolerable.[51] When intravenously injected, the iron oxide nanoparticles are typically degraded in liver and spleen, and subsequently incorporated into iron metabolic pathways.[52] Indeed, although the early generation SPION-based contrast agents for intravenous injection are no longer available in clinics, iron oxide nanoparticles are still used for the treatment of iron deficiency anemia[53] and for MRI of gastrointestinal tract via oral administration.[54]

Second, nanoparticle syntheses based on the thermal decomposition of metal complexes yield high-quality nanoparticles with tunable size and superior crystallinity.[23,55] As a result, the magnetic property of the nanoparticles can be controlled from nearly paramagnetic to ferromagnetic by tuning their size from a few to ~100 nm (Figure 2a,b). Such modulation of nanoparticle size allows the magnetic nanoparticles to be used either as a nontoxic alternative to Gd(III)-based T_1 contrast agents or as a highly sensitive T_2 contrast agent. For example, extremely small-sized iron oxide nanoparticles (ESIONs) less than 3 nm in core size exhibit a large T_1 contrast effect in high-resolution MR angiography.[38] On the other hand, ferrimagnetic iron oxide nanoparticles (FIONs) with a diameter larger than 30 nm enable highly sensitive T_2-weighted MRI of individual cells due to their strong magnetic property and facile cellular uptake.[56] In addition, FIONs with an average core size of 22 nm exhibit ~7 times stronger T_2 contrast effects than those of the first generation SPION-based agents predicted by outer-sphere relaxation theory.[21] Such a strong contrast effect can be attributed to the balance between the magnetization and the diffusion rate of the 22 nm-sized FIONs, which respectively are directly and inversely proportional to the nanoparticle size.[57] Moreover, it is also possible to control the MR contrast effect by changing the magnetic composition of nanoparticles. For instance, the addition of paramagnetic Gd^{3+} ions into iron oxide nanoparticles improves T_1 contrast effect due to the increased interactions between the Gd^{3+} ions and water molecules.[58] Likewise, manganese ferrite and zinc-doped ferrite nanoparticles show increased net magnetization, resulting in much stronger T_2 contrast effect.[22,59]

This situation brings up a question: is it still worth pursuing nanoparticle-based MRI contrast agents? To deal with this question, it is necessary to consider various factors including safety, efficacy, and market shares.

Third, while modification of Gd(III) complexes usually requires complicated multistep organic reactions, the surface of nanoparticles can be modified relatively easily using conventional bioconjugate chemistry with various functional molecules.[60] Since the interactions between biological tissues and nanoparticles are mainly determined by the surface characteristics of the nanoparticles, biodistribution and cellular uptake of the nanoparticles can be readily controlled by the surface modification.[44] Furthermore, conjugation of targeting ligands allows more accurate diagnosis by providing information on the biological processes of interest.[61] To date, various targeting ligands including antibodies,[62] aptamers,[63] folic acid,[64] and Arg-Gly-Asp (RGD) peptide[65] have been studied for tumor

DOI: 10.1021/acscentsci.7b00574
ACS Cent. Sci. 2018, 4, 324−336

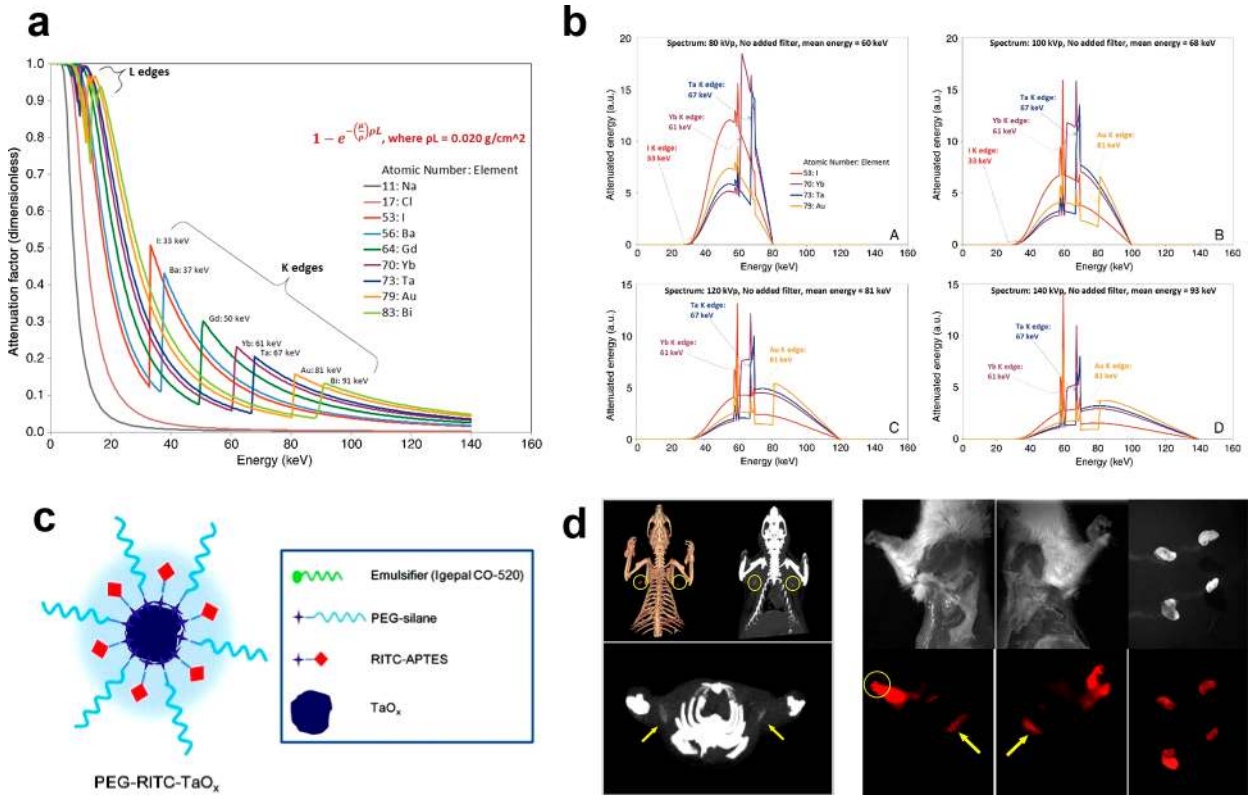

Figure 3. (a) X-ray attenuation factors of various elements. (b) Simulated attenuations of I, Yb, Ta, and Au against X-ray produced at 80 kVp (A), 100 kVp (B), 120 kVp (C), and 140 kVp (D). (c) Schematic illustration of RITC-doped tantalum oxide nanoparticles for multimodal imaging. (d) *In vivo* CT images (left) and optical images (right) of the sentinel lymph node of the rat 2 h after intradermal injection of RITC-doped tantalum oxide nanoparticles in both paws. Reprinted with permission from refs 29 and 82. Copyright 2011 American Chemical Society and 2015 RSNA.

diagnosis, leading to more enhanced binding affinity and specificity. In addition to the targeting ligands, various functional molecules such as fluorescence dyes, radioisotopes, and drugs can also be attached to the nanoparticles, which allows multimodal imaging or simultaneous imaging and therapy (referred to as theragnosis).[66]

As described above, there is still enormous potential in the nanoparticle-based MRI contrast agents, and new trials for more sensitive MR imaging are in progress. One of the challenging issues in the development of MR contrast agents lies in overcoming the intrinsic limitations of MRI such as low sensitivity and artifact signals. For example, either hyperintense or hypointense signal can be generated from endogenous factors such as fat, air, bleeding, calcification, or metal deposition, and they are sometimes confused with MR signals generated by contrast agents.[34] To address this issue, T_1−T_2 dual-mode MRI contrast agents have been introduced by combining superparamagnetic nanoparticles with paramagnetic metal ions (Figure 2c).[67] The dual-mode contrast agents generate bright and dark signals in T_1- and T_2-weighted MRI, respectively, enabling the intrinsic ambiguities to be overcome. In addition, sensitivity and accuracy of MRI can be improved by obtaining complementary information using multimodal imaging.[68] Therefore, various methods of preparing multimodal imaging probes have been proposed, including the direct conjugation of fluorescent molecules or radioisotopes,[69] the assembly of magnetic nanoparticles with quantum dots (QDs) or upconversion nanoparticles (UCNPs),[70] and the doping of radioisotopes into magnetic nanoparticles.[71]

Another challenging issue is designing the way that MR contrast agents respond to the stimuli of surrounding environments such as pH, temperature, and specific enzymes. For the case of Gd(III)-complex MR contrast agents, conformational changes of their chelate structures in response to various stimuli have been proposed.[72] In contrast, there have been scarce reports on the stimuli-responsive nanoparticle-based MR contrast agents because a magnetic field generated by superparamagnetic nanoparticles is not affected by conformational change of ligands, making the contrast effect "always on". On the other hand, clustering of the magnetic nanoparticles can change the T_2 relaxation rate, which is referred to as magnetic relaxation switch (MRS).[73] Because the aggregation of nanoparticles can be induced by specific interactions with specific target molecules, various small molecules including oligonucleotides, enzymes, and drugs are detected by MRS using MRI scanners and NMR spectrometers.[61] However, *in vivo* MRS remains very challenging as signal attenuation depends on the nanoparticle concentration as well as the degree of clustering. Recently, it is shown that extremely small iron oxide nanoparticles assembled within pH-responsive polymers can activate the MR signals in acidic conditions (Figure 2d).[74] When the nanoparticles are aggregated, strong T_2 contrast effect prevents T_1 contrast effect. However, the disassembly of the nanoparticles in acidic condition leads to increase in r_1 and decrease in r_2, which results in signal enhancement in T_1-weighted MRI.

Although magnetic nanoparticles are not currently available as MR contrast agents for systemic delivery, much attention and effort has been made to develop superior nanoparticle-

DOI: 10.1021/acscentsci.7b00574
ACS Cent. Sci. 2018, 4, 324−336

based contrast agents that hold great promise to provide enhanced sensitivity and more accurate diagnosis. Besides MR contrast agents based on iron oxide nanoparticles, lanthanide ion-doped nanoparticles are also strong candidates for novel MRI contrast agents. For example, $NaGdF_4$ nanoparticles have been developed as multimodal imaging agents for T_1-weighted MRI, CT, and upconversion imaging.[75] In addition, Dy^{3+} and Ho^{3+} ions exhibit unique magnetic characteristics such as short electronic relaxation time and large magnetic moment, which are suitable for high-field MRI.[76] Although high-field MRI improves the resolution and sensitivity, the contrast effect of iron oxide nanoparticles is marginally increased because their magnetization is already saturated. On the other hand, the magnetization of Dy^{3+} and Ho^{3+} is not saturated at the high magnetic field, making $NaHoF_4$ and $NaDyF_4$ good candidates for a T_2 contrast agent for high-field MRI. Furthermore, it is expected that optimized contrast effect can be obtained by modulating particle size, surface coating, and magnetic field.

CT CONTRAST AGENTS

Computed tomography (CT) is a medical imaging procedure based on the interaction of X-ray with a body or a contrast agent.[18] While rotating an X-ray tube and a detector, the intensity of X-ray is measured from different angles, and cross-sectional (tomographic) images are generated with the aid of a computer using the X-ray intensity profiles. CT is one of the most widely used whole body imaging techniques owing to its high spatial resolution and rapid image acquisition. As such, it is frequently employed to visualize various anatomical structures, including brain, lung, cardiovascular system, and abdominal diseases. The innate sensitivity of CT is not sufficiently high for most applications, and thus contrast agents are often required to detect a subtle change of soft tissues. Approximately half of the CT scans in clinics are aided by contrast agents.[77]

Since the X-ray attenuation effect of a material generally increases with its atomic number, high-Z elements are preferred as CT contrast agents.[78] To date, barium- and iodine-based contrast agents have been used in clinical situations. Because CT can detect approximately 10^{-2} M concentration of a contrast agent,[79] a high dose should be administered, which raises a concern about the toxicity of the contrast agents. For example, although barium sulfate suspension has been administered via oral route for gastrointestinal imaging for decades, it cannot be used as an intravascular contrast agent due to its renal and cardiovascular toxicity.[80] Iodine-based small molecules such as iopamidol and iodixanol were approved as intravenous CT contrast agents by the Food and Drug Administration of the United States. There are still several concerns regarding the safety of the iodinated contrast agents such as allergic reaction and renal toxicity.[81] In addition, the blood circulation time of the iodinated contrast agents is very short, preventing their preferential accumulation in a lesion.

Besides toxicity and pharmacokinetics, barium- and iodine-based CT contrast agents do not exhibit sufficient CT contrast effect at higher X-ray tube voltages.[82] This is because the X-ray attenuation effect of an element sharply increases at its K-edge energy level, and subsequently decreases at higher energy levels (Figure 3a).[83] Many of the current CT scanners are operated at tube voltages ranging from 80 to 140 kV, and high voltages are usually used for large or obese patients. Given that the K-edge energy levels of iodine and barium are 33.2 and 37.4 keV,[83] respectively, there is a large mismatch between the energy required for the peak attenuation and the average energy of X-ray photons emitted from the high voltage tubes. For elements that have too high K-edge energy levels such as gold (80.7 keV) or bismuth (90.5 keV), their contrast effects are not very strong either, because the majority of the emitted X-ray photons generated by current tubes have lower energy than the K-edge levels of those elements.[82] It is noteworthy that polychromatic X-ray is generated in an X-ray tube, and the tube voltage represents the maximum energy of the generated X-ray photons. Therefore, the contrast effect of an element should be evaluated in a wide range of X-ray energies rather than by an attenuation coefficient at a single energy level (Figure 3b). Recent reports show that materials with intermediate K-edge levels such as ytterbium (K-edge at 61.3 keV) and tantalum (K-edge at 67.4 keV) exhibit higher CT contrast effect compared with iodine.[82]

Besides MR contrast agents based on iron oxide nanoparticles, lanthanide ion-doped nanoparticles are also strong candidates for novel MRI contrast agents.

Last but not least, the market price of the CT contrast agents is also a critical factor for the regular use of CT in clinics because a large amount of dose is typically required for each scanning session. For example, although the gold-based CT contrast agents are attractive as an alternative to iodinated contrast agents owing to their good biocompatibility and facile synthesis,[24,25] roughly 50 g of gold is consumed for each whole body scanning session, which makes the clinical use of gold-based CT contrast agents almost unrealistic in terms of cost. Lanthanides such as ytterbium can be cheaper alternatives, but the industrial production scale of lanthanides is not large enough to provide a sufficient amount of CT contrast agents.[84]

Although the radiation dose of CT is a great concern,[85] this does not lower the importance of the contrast agents. By virtue of its fast scan speed, wide availability, and low cost, CT is still the most popular imaging tool. Various CT scanning methods and image reconstruction techniques have been actively developed to overcome current limitations.[86−88] Since contrast agents allow higher conspicuity of images, it is anticipated that optimized contrast agents will reduce both the radiation exposure and the administered dose, leading to safer imaging. In conjunction with novel imaging techniques, the optimized contrast agents also would enable new diagnostic capabilities of CT by providing molecular and cellular information in addition to simple anatomical details.[9] For example, nanoparticles of high-Z elements have been used for imaging of blood vessels,[25] tumors,[27] transplanted cells,[89] and atherosclerosis.[88] Furthermore, development of lanthanide-based imaging[75] (e.g., upconversion optical imaging and T_1-weighted MRI) and conjugation of fluorescence dyes allow multimodal imaging (Figure 3c).[29] These multifunctional nanoparticles are expected to lead to more accurate diagnosis and facile treatment by combination image-guided procedures (Figure 3d). Unlike other imaging modalities, CT imaging typically requires a large amount of contrast agents owing to its low sensitivity, which may cause serious side effects. Although most reports on CT contrast agent based on high-Z elements have stated that the nanoparticles are safe, their long-term toxicity has yet to be elucidated. For successful translation into clinical use, it is

DOI: 10.1021/acscentsci.7b00574
ACS Cent. Sci. 2018, 4, 324−336

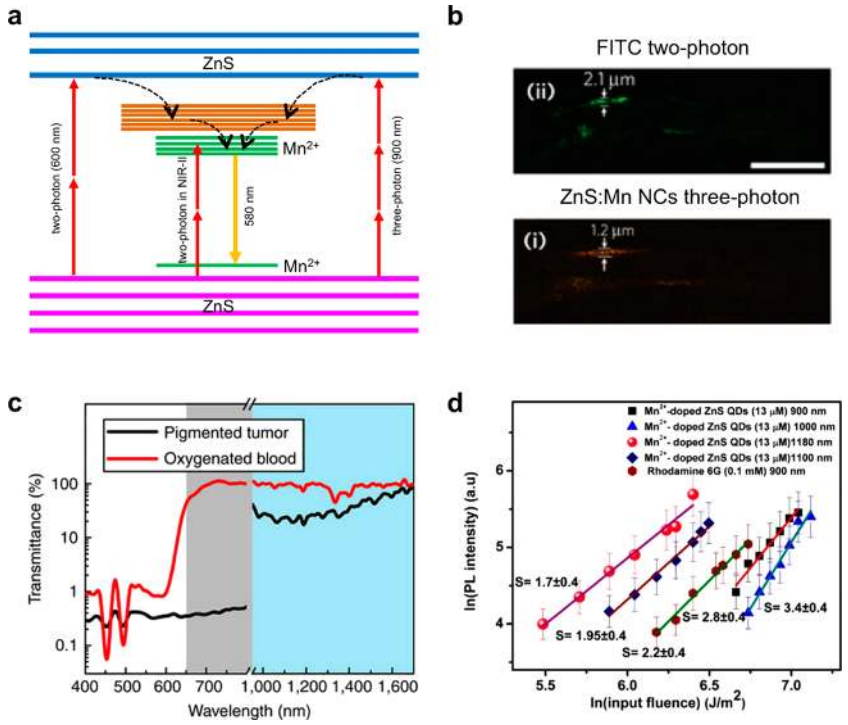

Figure 4. (a) Energy diagram of ZnS:Mn nanoparticles excited by multiphoton absorption. Two-photon absorption of ZnS (600 nm) or Mn^{2+} (NIR-II region) induces orange emission. Three-photon absorption of ZnS also induces orange emission. (b) Two-photon image of FITC and three-photon image of ZnS:Mn nanoparticles. Three-photon imaging showed better spatial resolution. (c) Transmission spectra of tumor tissue and blood. The NIR-II region exhibits improved transmission. (d) PL intensity of ZnS:Mn nanoparticles at different excitation wavelengths. For comparison, Rhodamine 6G is measured at 900 nm. *S* is the slope of the linear fitting. Between 900 and 1000 nm, the excitation mechanism is a three-photon absorption, and between 1100 and 1180 nm, the excitation mechanism is switched to two-photon absorption. The efficiency of PL is highest when excited at 1180 nm. Reprinted with permission from refs 42, 97, and 101. Copyright 2013 Macmillan Publishers Limited and 2013 American Chemical Society.

desirable to develop the optimized nanoparticles with favorable biodistribution profile, while maintaining rapid excretion.

MULTIPHOTON FLUORESCENCE IMAGING PROBES

While whole-body imaging techniques such as MRI and CT play an important role in medical imaging owing to their high resolution and superior penetration depth, their long acquisition time prevents their practical use in real-time monitoring. Fluorescence imaging can be used to overcome such limitations. In general, fluorescence imaging is capable of obtaining high temporal and spatial resolution with good sensitivity.[90,91] The utility of *in vivo* fluorescence imaging for live animals, however, has been hampered by the shallow penetration depth of light in tissues and decreased spatial resolution that comes from light scattering. For this reason, there have been demands for the development of innovative fluorescence imaging probes and techniques. One of the recent examples of progress in this field is utilizing the anti-Stokes emission process that generates emission light with a shorter wavelength than that of the excitation light.[92,93] If combined with near-infrared (NIR) excitation sources, increased tissue penetration depth, as well as reduced background autofluorescence or light scattering, can be achieved.[94]

Multiphoton absorption is a well-known anti-Stokes emission process that has a potential to reduce both the photoinduced damage of samples and photobleaching of fluorophores.[92] Unfortunately, most small molecule-based multiphoton fluorescent dyes still suffer from their low photostability that prevents repeated excitation and prolonged imaging. Therefore, inorganic nanoparticle-based multiphoton fluorescence probes are studied as an alternative due to their improved resistance to photobleaching and relatively facile surface modification with functional molecules. Especially, semiconducting QDs are very attractive in that their emission spectra are tunable and their multiphoton absorption cross sections are much larger than those of traditional fluorescent dyes.[95] There are several other issues that need to be considered to fully make use of the potential of the QD-based multiphoton fluorescence probes in bioimaging, most notably safety and imaging efficiency.

While cadmium-containing QDs such as CdSe/CdS/ZnS core−shell nanoparticles have been demonstrated as a two-photon imaging probe, potential toxicity from cadmium is a major concern. To address this issue, cadmium-free QDs have been studied.[96−98] For example, manganese-doped ZnS (ZnS:Mn) nanoparticles have been used in multiphoton imaging.[97] Besides their low toxicity, the manganese dopants change the emission wavelength from ∼430 nm to ∼580 nm, allowing more light to escape from the tissues. The large three-photon absorption cross section of ZnS:Mn nanoparticles, which is 4 orders of magnitude larger than those of ultraviolet (UV) fluorescent dyes, enables the three-photon excitation by 920 nm NIR laser, allowing deeper tissue penetration compared with two-photon imaging (Figure 4a). Spatial resolution is also much improved due to the reduced out-of-focus excitation and diminished background fluorescence (Figure 4b). Other than the ZnS:Mn nanoparticles, InP/ZnS[99] or $CuInS_2$/ZnS QDs[100] are also promising candidates for less-toxic probes.

DOI: 10.1021/acscentsci.7b00574
ACS Cent. Sci. 2018, 4, 324−336

As described earlier, the multiphoton excitation of QDs using NIR laser presents a number of advantages over UV excitation of fluorescent dye, although light scattering from biological tissues remains a problem that limits the fluorescence imaging of deep tissues. To further minimize the light scattering, the second near-infrared (NIR-II) range (1000 to 1700 nm) has been suggested as a better optical window (Figure 4c).[41,42] For instance, ZnS:Mn QDs, which were previously described as a three-photon imaging probe, were shown to have a superior two-photon imaging characteristic under NIR-II excitation (Figure 4d).[101] Compared with the two-photon excitation of ZnS host using a 600 nm laser, direct two-photon excitation of the manganese dopants by a 1050−1310 nm light source can benefit from the large two-photon absorption cross section of the manganese ions and deeper light penetration depth of the NIR-II window. However, the quantum efficiencies of QDs by NIR or NIR-II multiphoton excitation are still very low. The emission light from the QDs is also subjected to the absorption and scattering by the tissues, which further reduces the imaging quality. Finally, multiphoton imaging requires a microscope equipped with an expensive high-power femtosecond pulsed laser as an excitation source, and the laser beam should be focused for scanning, which delays the data acquisition. Therefore, the development of QDs with high multiphoton quantum efficiency as well as the development of imaging techniques for rapid acquisition of high-resolution images is urgent for the wide application of multiphoton imaging.

LUMINESCENCE UPCONVERSION IMAGING PROBES

Upconversion is another mechanism of the anti-Stokes emission processes, and it has received much attention in recent years to develop novel luminescent probes.[93] Similar to the multiphoton absorption, a NIR excitation source can be used for deeper light penetration and minimal background autofluorescence. Compared with the multiphoton absorption, however, the upconversion mechanism involves the photon absorption through real electronic intermediate states, resulting in a much higher emission efficiency and a longer luminescence lifetime up to several hundred microseconds.[102,103] Therefore, UCNPs can be excited at a low-power density using a continuous-wave laser diode. As such, image scanning by the focused pulsed laser is not necessary, and data acquisition can be performed much faster using wide-field microscopy.[104−107]

> Since the nanoparticle probes are usually composed of various inorganic elements and organic molecules for core material and surface coating, respectively, individual components can be tailored for specific applications.

Unlike the QDs, the emission wavelength of lanthanide-doped inorganic UCNPs is not related to the quantum confinement effect but dependent on the energy levels of individual lanthanide elements.[108,109] Therefore, emission color tuning is achieved by controlling the elemental composition of the UCNPs.[110,111] Luminescence lifetime is also tunable from several to thousands of microseconds by changing the type or the percentage of dopants,[103] which allows multiplex imaging not only by different emission colors but also by different lifetimes. The long luminescence lifetime of the UCNPs is also beneficial to the time-gated fluorescence imaging, where increased image contrast is obtained by separating the UCNP emission from light scattering.[112]

Although the upconversion efficiency of the lanthanide-doped inorganic UCNPs is exceeded by those of the organic dye-based UCNPs that use triplet−triplet annihilation upconversion,[113,114] it has been shown that the photon collection efficiency can be enhanced by functionalizing the lanthanide-doped inorganic UCNPs with antenna materials such as NIR dyes (Figure 5a),[115−118] gold nanoshells,[70] or QDs.[119] These antennas can also expand the range of absorption wavelength, allowing the flexible choice of excitation sources. In addition, more robust chemical stability and photostability of the inorganic UCNPs than those of the upconverting organic dyes in aqueous or air condition render them better suited for bioimaging applications. Further efforts to enhance the emission efficiency of the lanthanide-doped inorganic UCNPs include the controlled doping of core−shell structured UCNPs with different lanthanide dopants to facilitate the energy transfer,[102] and the high-irradiance excitation of UCNPs, where the luminescence quenching of the dopant ions is alleviated by the strong excitation power.[120]

While UCNPs are promising as a new luminescence imaging probe, it is important to point out the current limitations of the UCNPs. First of all, limited tunability of the emission wavelength can restrict the multiplex imaging. Because of the ladder-like energy levels of the lanthanide emitters, there are always multiple emission peaks. For example, erbium ions generate green and red emission, and thulium ions are known to exhibit UV, blue, and NIR emission.[121] Although there have been several reports on obtaining pure emission colors from UCNPs, especially for red, emission wavelength tuning is still a challenging issue that requires further exploration.[122,123]

Another issue is the heating effect by 980 nm NIR laser, which is usually used for the excitation of many types of UCNPs. Since water molecules can absorb the photons of the incident 980 nm laser, their temperature may increase. This heating effect may not be noticeable in most cellular imaging situations.[104] However, the high-power laser used for *in vivo* imaging may induce a thermal change large enough to affect the upconversion luminescence properties of the UCNPs and possibly cause damage to tissues. To minimize the heating effect, alternative excitation wavelengths whose energies are less absorbed by water molecules have been sought.[124] In a recent study, Nd^{3+} ions were introduced to UCNPs as a new sensitizer dopant that can be excited at 800 nm with marginal heating effect (Figure 5b).[125−127] Further research on various combinations of sensitizer and host materials is clearly needed to develop an optimized system for clinical use.

UCNPs are not free from the biosafety issues. Since an increasing number of UCNPs are now studied for *in vivo* applications, careful evaluation of their potential toxic effects is of great importance. To date, several systematic studies have been made to investigate the *in vivo* toxicity of UCNPs in mice,[128−132] zebrafish embryos,[133,134] and *Caenorhabditis elegans* worms,[135−137] and many results suggest little to no toxicity with small doses (e.g., <1 mg/kg). UCNPs indeed can be regarded as safer than the cadmium-containing QDs, but they are not completely safe as an overdose of UCNPs still can induce a severe toxicity. Consequently, the administration of UCNPs for bioimaging should be kept as minimal as possible,

DOI: 10.1021/acscentsci.7b00574
ACS Cent. Sci. 2018, 4, 324−336

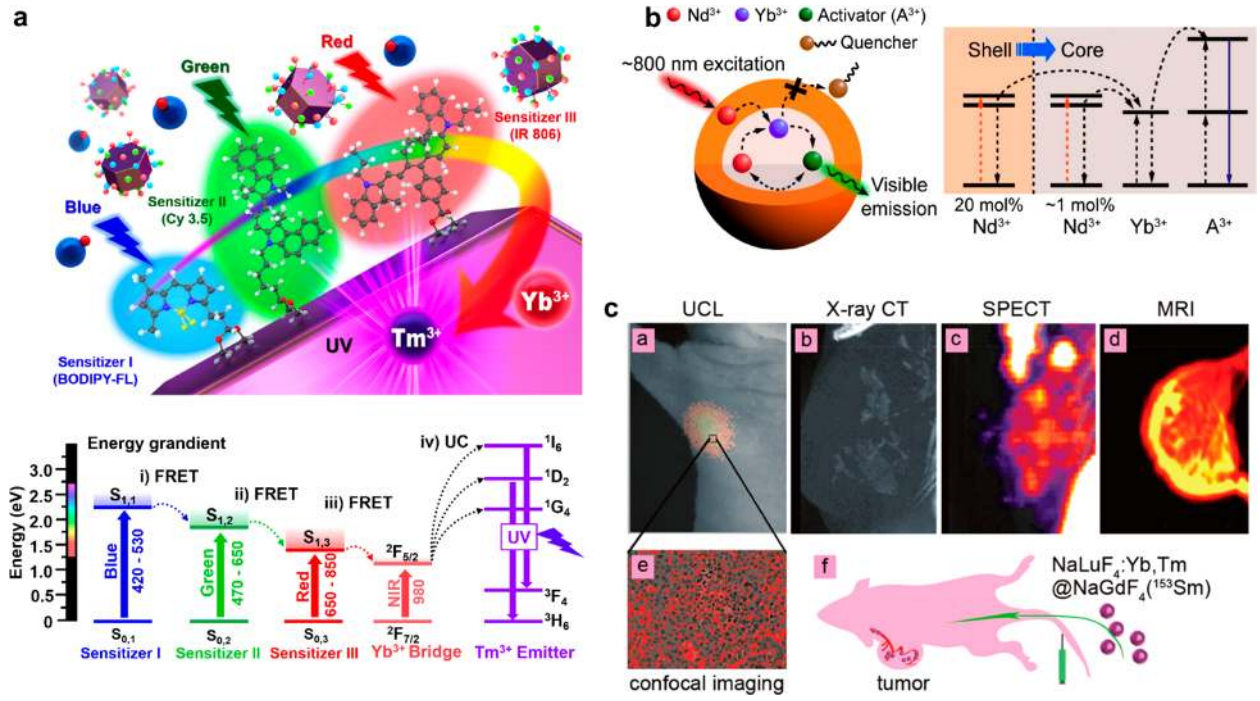

Figure 5. (a) Left: The schematic of multi-dye-sensitized UCNPs for a broad range of light absorption. Three dye sensitizers (e.g., BODIPY-FL for blue absorption, Cy 3.5 for green absorption, and IR 806 for red absorption) are immobilized on the nanoparticles. Right: The energy diagram of the three sensitizers and the UCNPs. (b) Left: The schematic of Nd^{3+}-doped core/shell UCNPs excited under 800 nm irradiation. Right: The energy diagram of the core/shell UCNPs. (c) $NaLuF_4$:Yb,Tm@$NaGdF_4$ (^{153}Sm) nanoparticles work as a multimodal imaging agent for upconversion luminescence imaging (Yb^{3+},Tm^{3+}), CT (Lu^{3+},Yb^{3+}), T_1 MRI (Gd^{3+}), and SPECT ($^{153}Sm^{3+}$). Reprinted with permission from refs 117, 125, and 139. Copyright 2017 Wiley and 2013 American Chemical Society.

which again emphasizes the significance of developing efficient probes.

CONCLUSION

Various inorganic nanoparticles have been developed and used as probes for *in vivo* biomedical imaging. For MRI and CT, several nanoparticle-based contrast agents have been shown to outperform conventional small molecule-based contrast agents in terms of imaging quality. Moreover, they are less toxic and easier to functionalize with targeting or stimuli-responsive ligands for effective treatment. The use of QDs or UCNPs for optical imaging also works as a good alternative to the optical imaging by organic dyes. The higher photostability and the larger absorption cross section of the QDs and UCNPs endow *in vivo* imaging with high-resolution and good signal-to-noise ratio. Especially, imaging techniques based on the multiphoton or upconversion process can make use of NIR light to obtain the images of deeper tissues. Recently, photoacoustic imaging has also emerged as a promising imaging technique to provide centimeter penetration depth with micrometer resolution.[138] Even though photoacoustic imaging exhibits better tissue penetration capability than anti-Stokes shift-based luminescence imaging, simultaneous imaging of multiple targets is only allowed by luminescence multicolor imaging, which is an advantage of luminescence-based imaging.[111] Despite all these benefits, nanoparticle imaging probes are not yet ready to completely replace the conventional contrast agents or fluorescence/luminescence dyes. Future research should be aimed at improving the efficiencies of the imaging modalities as well as the nanoparticle probes.

It is also worth mentioning the possibilities of the nanoparticle probes for multifunctional capabilities. Since the nanoparticle probes are usually composed of various inorganic elements and organic molecules for core material and surface coating, respectively, individual components can be tailored for specific applications (Figure 5c).[139] For example, Gd^{3+} ions which exhibit T_1 MRI contrast effects can be doped into UCNPs to produce a luminescence/MRI dual-modal imaging probe. And, Lu^{3+} (or Yb^{3+}) ions of UCNPs which have high atomic numbers can show a higher CT contrast enhancement than iodinated ones. This kind of multimodal imaging strategy is quite useful because the advantages of each imaging modality, such as high sensitivity or high penetration depth, can be combined altogether. Moreover, multimodal imaging probes not only provide the means for complementary imaging of the same region of interest but also can enable the imaging of different regions by individual imaging techniques. As a result, more comprehensive and reliable diagnosis is possible with

Moreover, multimodal imaging probes not only provide the means for complementary imaging of the same region of interest but also can enable the imaging of different regions by individual imaging techniques. As a result, more comprehensive and reliable diagnosis is possible with smaller quantities of nanoparticle probes than those for separate imaging.

DOI: 10.1021/acscentsci.7b00574
ACS Cent. Sci. 2018, 4, 324−336

smaller quantities of nanoparticle probes than those for separate imaging. Judicious design is necessary, though, as simple integration without any specific purpose may not bring any synergistic effect. In addition to the combination of different imaging modalities, drug molecules can be incorporated onto the surface of the nanoparticle probes using bioconjugation chemistry, producing theranostic agents. There are still plenty of untapped possibilities for such combinations that remain to be realized.

As always, biosafety of inorganic nanoparticle probes is critical, and it should be assessed carefully to fully draw out the potentials of the nanoparticle probes in bioimaging. While several issues regarding the toxicity, biodistribution, and clearance of nanoparticles in living animals have been investigated for the past decade, our current understanding is still far from complete. A bottom line would be synthesizing nanoparticle probes using less toxic elements and green chemistry if possible. Surface functionality and the overall size of the nanoparticle probes, which are closely related to the physical properties of the nanoparticle probes, are also known to affect the circulation, uptake, distribution, and clearance properties *in vivo*. Therefore, it would be required to optimize various factors for the best *in vivo* results, since the nanoparticle probes with the highest physical performance do not always necessarily exhibit the greatest biological efficacy.

AUTHOR INFORMATION

Corresponding Authors

*E-mail: ypark@jnu.ac.kr.
*E-mail: nohyunlee@kookmin.ac.kr.
*E-mail: thyeon@snu.ac.kr.

ORCID

Jonghoon Kim: 0000-0002-9511-9850
Yong Il Park: 0000-0003-3167-4908
Nohyun Lee: 0000-0001-6296-2625

Notes

The authors declare no competing financial interest.

ACKNOWLEDGMENTS

T.H. is supported by the Research Center Program of the Institute for Basic Science (IBS) in Korea (IBS-R006-D1). N.L. is supported by Basic Science Research Program (2015R1C1A1A01053463) and Bio & Medical Technology Development Program (2017M3A9G5082642) through the National Research Foundation of Korea (NRF) funded by the Ministry of Science, ICT & Future Planning. Y.I.P. is supported by the National Research Foundation of Korea (NRF) grant funded by the Korea government (Ministry of Science, ICT & Future Planning) (No. 2016R1A4A1012224).

REFERENCES

(1) Kunjachan, S.; Ehling, J.; Storm, G.; Kiessling, F.; Lammers, T. Noninvasive Imaging of Nanomedicines and Nanotheranostics: Principles, Progress, and Prospects. *Chem. Rev.* **2015**, *115*, 10907−10937.

(2) Kircher, M. F.; Willmann, J. K. Molecular Body Imaging: MR Imaging, CT, and US. Part I. Principles. *Radiology* **2012**, *263*, 633−643.

(3) Kobayashi, H.; Longmire, M. R.; Ogawa, M.; Choyke, P. L. Rational Chemical Design of the Next Generation of Molecular Imaging Probes Based on Physics and Biology: Mixing Modalities, Colors and Signals. *Chem. Soc. Rev.* **2011**, *40*, 4626.

(4) Pan, D.; Roessl, E.; Schlomka, J.-P.; Caruthers, S. D.; Senpan, A.; Scott, M. J.; Allen, J. S.; Zhang, H.; Hu, G.; Gaffney, P. J.; Choi, E. T.; Rasche, V.; Wickline, S. A.; Proksa, R.; Lanza, G. M. Computed Tomography in Color: NanoK-Enhanced Spectral CT Molecular Imaging. *Angew. Chem., Int. Ed.* **2010**, *49*, 9635−9639.

(5) Barrow, M.; Taylor, A.; Murray, P.; Rosseinsky, M. J.; Adams, D. J. Design Considerations for the Synthesis of Polymer Coated Iron Oxide Nanoparticles for Stem Cell Labelling and Tracking Using MRI. *Chem. Soc. Rev.* **2015**, *44*, 6733−6748.

(6) Ni, D.; Zhang, J.; Bu, W.; Xing, H.; Han, F.; Xiao, Q.; Yao, Z.; Chen, F.; He, Q.; Liu, J.; Zhang, S.; Fan, W.; Zhou, L.; Peng, W.; Shi, J. Dual-Targeting Upconversion Nanoprobes across the Blood−Brain Barrier for Magnetic Resonance/Fluorescence Imaging of Intracranial Glioblastoma. *ACS Nano* **2014**, *8*, 1231−1242.

(7) Rieffel, J.; Chen, F.; Kim, J.; Chen, G.; Shao, W.; Shao, S.; Chitgupi, U.; Hernandez, R.; Graves, S. A.; Nickles, R. J.; Prasad, P. N.; Kim, C.; Cai, W.; Lovell, J. F. Hexamodal Imaging with Porphyrin-Phospholipid-Coated Upconversion Nanoparticles. *Adv. Mater.* **2015**, *27*, 1785−1790.

(8) Cai, E.; Ge, P.; Lee, S. H.; Jeyifous, O.; Wang, Y.; Liu, Y.; Wilson, K. M.; Lim, S. J.; Baird, M. A.; Stone, J. E.; Lee, K. Y.; Davidson, M. W.; Chung, H. J.; Schulten, K.; Smith, A. M.; Green, W. N.; Selvin, P. R. Stable Small Quantum Dots for Synaptic Receptor Tracking on Live Neurons. *Angew. Chem., Int. Ed.* **2014**, *53*, 12484−12488.

(9) Motiei, M.; Dreifuss, T.; Betzer, O.; Panet, H.; Popovtzer, A.; Santana, J.; Abourbeh, G.; Mishani, E.; Popovtzer, R. Differentiating between Cancer and Inflammation: A Metabolic-Based Method for Functional Computed Tomography Imaging. *ACS Nano* **2016**, *10*, 3469−3477.

(10) Ghosh, D.; Lee, Y.; Thomas, S.; Kohli, A. G.; Yun, D. S.; Belcher, A. M.; Kelly, K. A. M13-Templated Magnetic Nanoparticles for Targeted *in vivo* Imaging of Prostate Cancer. *Nat. Nanotechnol.* **2012**, *7*, 677−682.

(11) Aime, S.; Castelli, D. D.; Crich, S. G.; Gianolio, E.; Terreno, E. Pushing the Sensitivity Envelope of Lanthanide-Based Magnetic Resonance Imaging (MRI) Contrast Agents for Molecular Imaging Applications. *Acc. Chem. Res.* **2009**, *42*, 822−831.

(12) Singh, J.; Daftary, A. Iodinated Contrast Media and Their Adverse Reactions. *J. Nucl. Med. Technol.* **2008**, *36*, 69−74 (quiz 76−7).

(13) Choi, H. S.; Nasr, K.; Alyabyev, S.; Feith, D.; Lee, J. H.; Kim, S. H.; Ashitate, Y.; Hyun, H.; Patonay, G.; Strekowski, L.; Henary, M.; Frangioni, J. V. Synthesis and in vivo Fate of Zwitterionic Near-Infrared Fluorophores. *Angew. Chem., Int. Ed.* **2011**, *50*, 6258−6263.

(14) Wu, X.; Liu, H.; Liu, J.; Haley, K. N.; Treadway, J. A.; Larson, J. P.; Ge, N.; Peale, F.; Bruchez, M. P. Immunofluorescent Labeling of Cancer Marker Her2 and Other Cellular Targets with Semiconductor Quantum Dots. *Nat. Biotechnol.* **2003**, *21*, 41−46.

(15) Hadjipanayis, C. G.; Bonder, M. J.; Balakrishnan, S.; Wang, X.; Mao, H.; Hadjipanayis, G. C. Metallic Iron Nanoparticles for MRI Contrast Enhancement and Local Hyperthermia. *Small* **2008**, *4*, 1925−1929.

(16) Mi, P.; Kokuryo, D.; Cabral, H.; Wu, H.; Terada, Y.; Saga, T.; Aoki, I.; Nishiyama, N.; Kataoka, K. A pH-Activatable Nanoparticle with Signal-Amplification Capabilities for Non-Invasive Imaging of Tumour Malignancy. *Nat. Nanotechnol.* **2016**, *11*, 724−730.

(17) Lee, N.; Yoo, D.; Ling, D.; Cho, M. H.; Hyeon, T.; Cheon, J. Iron Oxide Based Nanoparticles for Multimodal Imaging and Magnetoresponsive Therapy. *Chem. Rev.* **2015**, *115*, 10637−10689.

(18) Lee, N.; Choi, S. H.; Hyeon, T. Nano-Sized CT Contrast Agents. *Adv. Mater.* **2013**, *25*, 2641−2660.

(19) Park, Y. I.; Lee, K. T.; Suh, Y. D.; Hyeon, T. Upconverting Nanoparticles: A Versatile Platform for Wide-Field Two-Photon Microscopy and Multi-Modal in Vivo Imaging. *Chem. Soc. Rev.* **2015**, *44*, 1302−1317.

(20) Giljohann, D. A.; Seferos, D. S.; Daniel, W. L.; Massich, M. D.; Patel, P. C.; Mirkin, C. A. Gold Nanoparticles for Biology and Medicine. *Angew. Chem., Int. Ed.* **2010**, *49*, 3280−3294.

DOI: 10.1021/acscentsci.7b00574
ACS Cent. Sci. 2018, 4, 324−336

(21) Lee, N.; Choi, Y.; Lee, Y.; Park, M.; Moon, W. K.; Choi, S. H.; Hyeon, T. Water-Dispersible Ferrimagnetic Iron Oxide Nanocubes with Extremely High R_2 Relaxivity for Highly Sensitive in vivo MRI of Tumors. *Nano Lett.* **2012**, *12*, 3127−3131.
(22) Jang, J.-t.; Nah, H.; Lee, J.-H.; Moon, S. H.; Kim, M. G.; Cheon, J. Critical Enhancements of MRI Contrast and Hyperthermic Effects by Dopant-Controlled Magnetic Nanoparticles. *Angew. Chem., Int. Ed.* **2009**, *48*, 1234−1238.
(23) Chen, R.; Christiansen, M. G.; Sourakov, A.; Mohr, A.; Matsumoto, Y.; Okada, S.; Jasanoff, A.; Anikeeva, P. High-Performance Ferrite Nanoparticles through Nonaqueous Redox Phase Tuning. *Nano Lett.* **2016**, *16*, 1345−1351.
(24) Hainfeld, J. F.; Slatkin, D. N.; Focella, T. M.; Smilowitz, H. M. Gold Nanoparticles: A New X-Ray Contrast Agent. *Br. J. Radiol.* **2006**, *79*, 248−253.
(25) Kim, D.; Park, S.; Lee, J. H.; Jeong, Y. Y.; Jon, S. Antibiofouling Polymer-Coated Gold Nanoparticles as a Contrast Agent for in vivo X-Ray Computed Tomography Imaging. *J. Am. Chem. Soc.* **2007**, *129*, 7661−7665.
(26) Rabin, O.; Perez, J. M.; Grimm, J.; Wojtkiewicz, G.; Weissleder, R. An X-Ray Computed Tomography Imaging Agent Based on Long-Circulating Bismuth Sulphide Nanoparticles. *Nat. Mater.* **2006**, *5*, 118−122.
(27) Kinsella, J. M.; Jimenez, R. E.; Karmali, P. P.; Rush, A. M.; Kotamraju, V. R.; Gianneschi, N. C.; Ruoslahti, E.; Stupack, D.; Sailor, M. J. X-Ray Computed Tomography Imaging of Breast Cancer by Using Targeted Peptide-Labeled Bismuth Sulfide Nanoparticles. *Angew. Chem., Int. Ed.* **2011**, *50*, 12308−12311.
(28) Ai, K.; Liu, Y.; Liu, J.; Yuan, Q.; He, Y.; Lu, L. Large-Scale Synthesis of Bi_2S_3 Nanodots as a Contrast Agent for in Vivo X-Ray Computed Tomography Imaging. *Adv. Mater.* **2011**, *23*, 4886−4891.
(29) Oh, M. H.; Lee, N.; Kim, H.; Park, S. P.; Piao, Y.; Lee, J.; Jun, S. W.; Moon, W. K.; Choi, S. H.; Hyeon, T. Large-Scale Synthesis of Bioinert Tantalum Oxide Nanoparticles for X-Ray Computed Tomography Imaging and Bimodal Image-Guided Sentinel Lymph Node Mapping. *J. Am. Chem. Soc.* **2011**, *133*, 5508−5515.
(30) Bonitatibus, P. J., Jr.; Torres, A. S.; Goddard, G. D.; FitzGerald, P. F.; Kulkarni, A. M. Synthesis, Characterization, and Computed Tomography Imaging of a Tantalum Oxide Nanoparticle Imaging Agent. *Chem. Commun.* **2010**, *46*, 8956−8958.
(31) Gao, X.; Cui, Y.; Levenson, R. M.; Chung, L. W. K.; Nie, S. In vivo Cancer Targeting and Imaging with Semiconductor Quantum Dots. *Nat. Biotechnol.* **2004**, *22*, 969−976.
(32) Bruchez, M., Jr.; Moronne, M.; Gin, P.; Weiss, S.; Alivisatos, A. P. Semiconductor Nanocrystals as Fluorescent Biological Labels. *Science* **1998**, *281*, 2013−2016.
(33) Kim, S.; Lim, Y. T.; Soltesz, E. G.; De Grand, A. M.; Lee, J.; Nakayama, A.; Parker, J. A.; Mihaljevic, T.; Laurence, R. G.; Dor, D. M.; Cohn, L. H.; Bawendi, M. G.; Frangioni, J. V. Near-Infrared Fluorescent Type II Quantum Dots for Sentinel Lymph Node Mapping. *Nat. Biotechnol.* **2004**, *22*, 93−97.
(34) Bulte, J. W. M.; Kraitchman, D. L. Iron Oxide MR Contrast Agents for Molecular and Cellular Imaging. *NMR Biomed.* **2004**, *17*, 484−499.
(35) Mortensen, L. J.; Oberdoerster, G.; Pentland, A. P.; Delouise, L. A. In vivo Skin Penetration of Quantum Dot Nanoparticles in the Murine Model: The Effect of UVR. *Nano Lett.* **2008**, *8*, 2779−2787.
(36) Tsoi, K. M.; Dai, Q.; Alman, B. A.; Chan, W. C. W. Are Quantum Dots Toxic? Exploring the Discrepancy between Cell Culture and Animal Studies. *Acc. Chem. Res.* **2013**, *46*, 662−671.
(37) Ye, L.; Yong, K.-T.; Liu, L.; Roy, I.; Hu, R.; Zhu, J.; Cai, H.; Law, W.-C.; Liu, J.; Wang, K.; Liu, J.; Liu, Y.; Hu, Y.; Zhang, X.; Swihart, M. T.; Prasad, P. N. A Pilot Study in Non-Human Primates Shows No Adverse Response to Intravenous Injection of Quantum Dots. *Nat. Nanotechnol.* **2012**, *7*, 453−458.
(38) Kim, B. H.; Lee, N.; Kim, H.; An, K.; Park, Y. I.; Choi, Y.; Shin, K.; Lee, Y.; Kwon, S. G.; Na, H. B.; Park, J.-G.; Ahn, T.-Y.; Kim, Y.-W.; Moon, W. K.; Choi, S. H.; Hyeon, T. Large-Scale Synthesis of Uniform and Extremely Small-Sized Iron Oxide Nanoparticles for High-Resolution T_1 Magnetic Resonance Imaging Contrast Agents. *J. Am. Chem. Soc.* **2011**, *133*, 12624−12631.
(39) Shen, Z.; Wu, A.; Chen, X. Iron Oxide Nanoparticle Based Contrast Agents for Magnetic Resonance Imaging. *Mol. Pharmaceutics* **2017**, *14*, 1352−1364.
(40) Weissleder, R.; Ntziachristos, V. Shedding Light onto Live Molecular Targets. *Nat. Med.* **2003**, *9*, 123−128.
(41) Hong, G.; Lee, J. C.; Robinson, J. T.; Raaz, U.; Xie, L.; Huang, N. F.; Cooke, J. P.; Dai, H. Multifunctional *in vivo* Vascular Imaging Using near-Infrared II Fluorescence. *Nat. Med.* **2012**, *18*, 1841−1846.
(42) Naczynski, D. J.; Tan, M. C.; Zevon, M.; Wall, B.; Kohl, J.; Kulesa, A.; Chen, S.; Roth, C. M.; Riman, R. E.; Moghe, P. V. Rare-Earth-Doped Biological Composites as *in vivo* Shortwave Infrared Reporters. *Nat. Commun.* **2013**, *4*, 2199.
(43) Li, C.; Zhang, Y.; Wang, M.; Zhang, Y.; Chen, G.; Li, L.; Wu, D.; Wang, Q. *In vivo* Real-Time Visualization of Tissue Blood Flow and Angiogenesis Using Ag_2S Quantum Dots in the NIR-II Window. *Biomaterials* **2014**, *35*, 393−400.
(44) Biju, V. Chemical Modifications and Bioconjugate Reactions of Nanomaterials for Sensing, Imaging, Drug Delivery and Therapy. *Chem. Soc. Rev.* **2014**, *43*, 744−764.
(45) Brown, M. A.; Semelka, R. C. *MRI: Basic Principles and Applications*; Wiley: 2011.
(46) Modo, M. M. J.; Bulte, J. W. M. *Molecular and Cellular MR Imaging*; CRC Press: 2007.
(47) Wang, Y.-X. J. Superparamagnetic Iron Oxide Based MRI Contrast Agents: Current Status of Clinical Application. *Quant. Imaging Med. Surg.* **2011**, *1*, 35−40.
(48) Kiessling, F.; Mertens, M. E.; Grimm, J.; Lammers, T. Nanoparticles for Imaging: Top or Flop? *Radiology* **2014**, *273*, 10−28.
(49) Jun, Y. W.; Huh, Y.-M.; Choi, J. S.; Lee, J. H.; Song, H. T.; Kim, S.; Yoon, S.; Kim, K. S.; Shin, J. S.; Suh, J. S.; Cheon, J. Nanoscale Size Effect of Magnetic Nanocrystals and Their Utilization for Cancer Diagnosis Via Magnetic Resonance Imaging. *J. Am. Chem. Soc.* **2005**, *127*, 5732−5733.
(50) Penfield, J. G.; Reilly, R. F. What Nephrologists Need to Know About Gadolinium. *Nat. Clin. Pract. Nephrol.* **2007**, *3*, 654−668.
(51) Arami, H.; Khandhar, A.; Liggitt, D.; Krishnan, K. M. In vivo Delivery, Pharmacokinetics, Biodistribution and Toxicity of Iron Oxide Nanoparticles. *Chem. Soc. Rev.* **2015**, *44*, 8576−8607.
(52) Kolosnjaj-Tabi, J.; Javed, Y.; Lartigue, L.; Volatron, J.; Elgrabli, D.; Marangon, I.; Pugliese, G.; Caron, B.; Figuerola, A.; Luciani, N.; Pellegrino, T.; Alloyeau, D.; Gazeau, F. The One Year Fate of Iron Oxide Coated Gold Nanoparticles in Mice. *ACS Nano* **2015**, *9*, 7925−7939.
(53) Schwenk, M. H. Ferumoxytol: A New Intravenous Iron Preparation for the Treatment of Iron Deficiency Anemia in Patients with Chronic Kidney Disease. *Pharmacotherapy* **2010**, *30*, 70−79.
(54) Giovagnoni, A.; Fabbri, A.; Maccioni, F. Oral Contrast Agents in MRI of the Gastrointestinal Tract. *Adbom. Imaging* **2002**, *27*, 367−375.
(55) Park, J.; An, K.; Hwang, Y. S.; Park, J. G.; Noh, H. J.; Kim, J. Y.; Park, J. H.; Hwang, N. M.; Hyeon, T. Ultra-Large-Scale Syntheses of Monodisperse Nanocrystals. *Nat. Mater.* **2004**, *3*, 891−895.
(56) Lee, N.; Kim, H.; Choi, S. H.; Park, M.; Kim, D.; Kim, H.-C.; Choi, Y.; Lin, S.; Kim, B. H.; Jung, H. S.; Kim, H.; Park, K. S.; Moon, W. K.; Hyeon, T. Magnetosome-Like Ferrimagnetic Iron Oxide Nanocubes for Highly Sensitive MRI of Single Cells and Transplanted Pancreatic Islets. *Proc. Natl. Acad. Sci. U. S. A.* **2011**, *108*, 2662−2667.
(57) Gillis, P.; Moiny, F.; Brooks, R. A. On T_2-Shortening by Strongly Magnetized Spheres: A Partial Refocusing Model. *Magn. Reson. Med.* **2002**, *47*, 257−263.
(58) Zhou, Z.; Wang, L.; Chi, X.; Bao, J.; Yang, L.; Zhao, W.; Chen, Z.; Wang, X.; Chen, X.; Gao, J. Engineered Iron-Oxide-Based Nanoparticles as Enhanced T_1 Contrast Agents for Efficient Tumor Imaging. *ACS Nano* **2013**, *7*, 3287−3296.
(59) Lee, J.-H.; Huh, Y.-M.; Jun, Y.-W.; Seo, J.-w.; Jang, J.-t.; Song, H.-T.; Kim, S.; Cho, E.-J.; Yoon, H.-G.; Suh, J.-S.; Cheon, J. Artificially

DOI: 10.1021/acscentsci.7b00574
ACS Cent. Sci. 2018, 4, 324−336

Engineered Magnetic Nanoparticles for Ultra-Sensitive Molecular Imaging. *Nat. Med.* **2007**, *13*, 95−99.
(60) Laurent, S.; Forge, D.; Port, M.; Roch, A.; Robic, C.; Vander Elst, L.; Muller, R. N. Magnetic Iron Oxide Nanoparticles: Synthesis, Stabilization, Vectorization, Physicochemical Characterizations, and Biological Applications. *Chem. Rev.* **2008**, *108*, 2064−2110.
(61) Tassa, C.; Shaw, S. Y.; Weissleder, R. Dextran-Coated Iron Oxide Nanoparticles: A Versatile Platform for Targeted Molecular Imaging, Molecular Diagnostics, and Therapy. *Acc. Chem. Res.* **2011**, *44*, 842−852.
(62) Kievit, F. M.; Stephen, Z. R.; Veiseh, O.; Arami, H.; Wang, T.; Lai, V. P.; Park, J. O.; Ellenbogen, R. G.; Disis, M. L.; Zhang, M. Targeting of Primary Breast Cancers and Metastases in a Transgenic Mouse Model Using Rationally Designed Multifunctional Spions. *ACS Nano* **2012**, *6*, 2591−2601.
(63) Park, J.; Park, S.; Kim, S.; Lee, I.-H.; Saw, P. E.; Lee, K.; Kim, Y.-C.; Kim, Y.-J.; Farokhzad, O. C.; Jeong, Y. Y.; Jon, S. Her2-Specific Aptide Conjugated Magneto-Nanoclusters for Potential Breast Cancer Imaging and Therapy. *J. Mater. Chem. B* **2013**, *1*, 4576.
(64) Landmark, K. J.; DiMaggio, S.; Ward, J.; Kelly, C.; Vogt, S.; Hong, S.; Kotlyar, A.; Myc, A.; Thomas, T. P.; Penner-Hahn, J. E.; Baker, J. R.; Holl, M. M. B.; Orr, B. G. Synthesis, Characterization, and in Vitro Testing of Superparamagnetic Iron Oxide Nanoparticles Targeted Using Folic Acid-Conjugated Dendrimers. *ACS Nano* **2008**, *2*, 773−783.
(65) Zhang, F.; Huang, X.; Zhu, L.; Guo, N.; Niu, G.; Swierczewska, M.; Lee, S.; Xu, H.; Wang, A. Y.; Mohamedali, K. A.; Rosenblum, M. G.; Lu, G.; Chen, X. Noninvasive Monitoring of Orthotopic Glioblastoma Therapy Response Using RGD-Conjugated Iron Oxide Nanoparticles. *Biomaterials* **2012**, *33*, 5414−5422.
(66) Lee, D.-E.; Koo, H.; Sun, I.-C.; Ryu, J. H.; Kim, K.; Kwon, I. C. Multifunctional Nanoparticles for Multimodal Imaging and Theragnosis. *Chem. Soc. Rev.* **2012**, *41*, 2656−2672.
(67) Shin, T.-H.; Choi, J.-s.; Yun, S.; Kim, I.-S.; Song, H.-T.; Kim, Y.; Park, K. I.; Cheon, J. T_1 and T_2 Dual-Mode MRI Contrast Agent for Enhancing Accuracy by Engineered Nanomaterials. *ACS Nano* **2014**, *8*, 3393−3401.
(68) Shin, T.-H.; Choi, Y.; Kim, S.; Cheon, J. Recent Advances in Magnetic Nanoparticle-Based Multi-Modal Imaging. *Chem. Soc. Rev.* **2015**, *44*, 4501−4516.
(69) Yang, X.; Hong, H.; Grailer, J. J.; Rowland, I. J.; Javadi, A.; Hurley, S. A.; Xiao, Y.; Yang, Y.; Zhang, Y.; Nickles, R. J.; Cai, W.; Steeber, D. A.; Gong, S. cRGD-Functionalized, Dox-Conjugated, and ^{64}Cu-Labeled Superparamagnetic Iron Oxide Nanoparticles for Targeted Anticancer Drug Delivery and PET/MR Imaging. *Biomaterials* **2011**, *32*, 4151−4160.
(70) Cheng, L.; Yang, K.; Li, Y.; Chen, J.; Wang, C.; Shao, M.; Lee, S.-T.; Liu, Z. Facile Preparation of Multifunctional Upconversion Nanoprobes for Multimodal Imaging and Dual-Targeted Photothermal Therapy. *Angew. Chem., Int. Ed.* **2011**, *50*, 7385−7390.
(71) Chakravarty, R.; Valdovinos, H. F.; Chen, F.; Lewis, C. M.; Ellison, P. A.; Luo, H.; Meyerand, M. E.; Nickles, R. J.; Cai, W. Intrinsically Germanium-69-Labeled Iron Oxide Nanoparticles: Synthesis and in-vivo Dual-Modality PET/MR Imaging. *Adv. Mater.* **2014**, *26*, 5119−5123.
(72) Yu, J.; Martins, A. F.; Preihs, C.; Clavijo Jordan, V.; Chirayil, S.; Zhao, P.; Wu, Y.; Nasr, K.; Kiefer, G. E.; Sherry, A. D. Amplifying the Sensitivity of Zinc(II) Responsive MRI Contrast Agents by Altering Water Exchange Rates. *J. Am. Chem. Soc.* **2015**, *137*, 14173−14179.
(73) Perez, J. M.; Josephson, L.; O'Loughlin, T.; Högemann, D.; Weissleder, R. Magnetic Relaxation Switches Capable of Sensing Molecular Interactions. *Nat. Biotechnol.* **2002**, *20*, 816−820.
(74) Ling, D.; Park, W.; Park, S.-j.; Lu, Y.; Kim, K. S.; Hackett, M. J.; Kim, B. H.; Yim, H.; Jeon, Y. S.; Na, K.; Hyeon, T. Multifunctional Tumor pH-Sensitive Self-Assembled Nanoparticles for Bimodal Imaging and Treatment of Resistant Heterogeneous Tumors. *J. Am. Chem. Soc.* **2014**, *136*, 5647−5655.
(75) Ma, D.; Meng, L.; Chen, Y.; Hu, M.; Chen, Y.; Huang, C.; Shang, J.; Wang, R.; Guo, Y.; Yang, J. $NaGdF_4$:Yb^{3+}/Er^{3+}@$NaGdF_4$:Nd^{3+}@Sodium-Gluconate: Multifunctional and Biocompatible Ultrasmall Core−Shell Nanohybrids for UCL/MR/CT Multimodal Imaging. *ACS Appl. Mater. Interfaces* **2015**, *7*, 16257−16265.
(76) Zhang, X.; Blasiak, B.; Marenco, A. J.; Trudel, S.; Tomanek, B.; van Veggel, F. C. J. M. Design and Regulation of $NaHoF_4$ and $NaDyF_4$ Nanoparticles for High-Field Magnetic Resonance Imaging. *Chem. Mater.* **2016**, *28*, 3060−3072.
(77) Berrington de Gonzalez, A.; Kleinerman, R. A. CT Scanning: Is the Contrast Material Enhancing the Radiation Dose and Cancer Risk as Well as the Image? *Radiology* **2015**, *275*, 627−629.
(78) Yu, S.-B.; Watson, A. D. Metal-Based X-Ray Contrast Media. *Chem. Rev.* **1999**, *99*, 2353−2378.
(79) Galper, M. W.; Saung, M. T.; Fuster, V.; Roessl, E.; Thran, A.; Proksa, R.; Fayad, Z. A.; Cormode, D. P. Effect of Computed Tomography Scanning Parameters on Gold Nanoparticle and Iodine Contrast. *Invest. Radiol.* **2012**, *47*, 475−481.
(80) Choudhury, H.; Cary, R. *Barium and Barium Compounds*; World Health Organization: 2001.
(81) Stacul, F.; van der Molen, A. J.; Reimer, P.; Webb, J. A. W.; Thomsen, H. S.; Morcos, S. K.; Almén, T.; Aspelin, P.; Bellin, M.-F.; Clément, O.; Heinz- Peer, G. Contrast Induced Nephropathy: Updated ESUR Contrast Media Safety Committee Guidelines. *Eur. Radiol.* **2011**, *21*, 2527−2541.
(82) FitzGerald, P. F.; Colborn, R. E.; Edic, P. M.; Lambert, J. W.; Torres, A. S.; Bonitatibus, J. P. J.; Yeh, B. M. CT Image Contrast of High-Z Elements: Phantom Imaging Studies and Clinical Implications. *Radiology* **2016**, *278*, 723−733.
(83) Hubbell, J.; Seltzer, S. *NIST: X-Ray Mass Attenuation Coefficients*; US Department of Commerce: 1995.
(84) Emsley, J. *Nature's Building Blocks: An a-Z. Guide to the Elements*; Oxford University Press: 2001.
(85) Schenkman, L. Second Thoughts about CT Imaging. *Science* **2011**, *331*, 1002−1004.
(86) Bernstein, A. L.; Dhanantwari, A.; Jurcova, M.; Cheheltani, R.; Naha, P. C.; Ivanc, T.; Shefer, E.; Cormode, D. P. Improved Sensitivity of Computed Tomography Towards Iodine and Gold Nanoparticle Contrast Agents via Iterative Reconstruction Methods. *Sci. Rep.* **2016**, *6*, 26177.
(87) Manohar, N.; Reynoso, F. J.; Diagaradjane, P.; Krishnan, S.; Cho, S. H. Quantitative Imaging of Gold Nanoparticle Distribution in a Tumor-Bearing Mouse Using Benchtop X-Ray Fluorescence Computed Tomography. *Sci. Rep.* **2016**, *6*, 22079.
(88) Cormode, D. P.; Roessl, E.; Thran, A.; Skajaa, T.; Gordon, R. E.; Schlomka, J.-P.; Fuster, V.; Fisher, E. A.; Mulder, W. J. M.; Proksa, R.; Fayad, Z. A. Atherosclerotic Plaque Composition: Analysis with Multicolor CT and Targeted Gold Nanoparticles. *Radiology* **2010**, *256*, 774−782.
(89) Kim, T.; Lee, N.; Arifin, D. R.; Shats, I.; Janowski, M.; Walczak, P.; Hyeon, T.; Bulte, J. W. M. In Vivo Micro-CT Imaging of Human Mesenchymal Stem Cells Labeled with Gold-Poly-L-Lysine Nanocomplexes. *Adv. Funct. Mater.* **2017**, *27*, 1604213.
(90) Giepmans, B. N. G.; Adams, S. R.; Ellisman, M. H.; Tsien, R. Y. The Fluorescent Toolbox for Assessing Protein Location and Function. *Science* **2006**, *312*, 217−224.
(91) Kobayashi, H.; Ogawa, M.; Alford, R.; Choyke, P. L.; Urano, Y. New Strategies for Fluorescent Probe Design in Medical Diagnostic Imaging. *Chem. Rev.* **2010**, *110*, 2620−2640.
(92) Gamelin, D. R.; Güdel, H. U. Design of Luminescent Inorganic Materials: New Photophysical Processes Studied by Optical Spectroscopy. *Acc. Chem. Res.* **2000**, *33*, 235−242.
(93) Auzel, F. Upconversion and Anti-Stokes Processes with F and D Ions in Solids. *Chem. Rev.* **2004**, *104*, 139−173.
(94) Weissleder, R. A Clearer Vision for *in vivo* Imaging. *Nat. Biotechnol.* **2001**, *19*, 316−317.
(95) Larson, D. R.; Zipfel, W. R.; Williams, R. M.; Clark, S. W.; Bruchez, M. P.; Wise, F. W.; Webb, W. W. Water-Soluble Quantum Dots for Multiphoton Fluorescence Imaging in vivo. *Science* **2003**, *300*, 1434−1436.

DOI: 10.1021/acscentsci.7b00574
ACS Cent. Sci. 2018, 4, 324−336

(96) Deng, Z. T.; Tong, L.; Flores, M.; Lin, S.; Cheng, J. X.; Yan, H.; Liu, Y. High-Quality Manganese-Doped Zinc Sulfide Quantum Rods with Tunable Dual-Color and Multiphoton Emissions. *J. Am. Chem. Soc.* **2011**, *133*, 5389−5396.
(97) Yu, J. H.; Kwon, S.-H.; Petrášek, Z.; Park, O. K.; Jun, S. W.; Shin, K.; Choi, M.; Park, Y. I.; Park, K.; Na, H. B.; Lee, N.; Lee, D. W.; Kim, J. H.; Schwille, P.; Hyeon, T. High-Resolution Three-Photon Biomedical Imaging Using Doped ZnS Nanocrystals. *Nat. Mater.* **2013**, *12*, 359−366.
(98) Zhao, B.; Yao, Y.; Yang, K.; Rong, P.; Huang, P.; Sun, K.; An, X.; Li, Z.; Chen, X.; Li, W. Mercaptopropionic Acid-Capped Mn^{2+}:ZnSe/ZnO Quantum Dots with Both Downconversion and Upconversion Emissions for Bioimaging Applications. *Nanoscale* **2014**, *6*, 12345−12349.
(99) Bharali, D. J.; Lucey, D. W.; Jayakumar, H.; Pudavar, H. E.; Prasad, P. N. Folate-Receptor-Mediated Delivery of InP Quantum Dots for Bioimaging Using Confocal and Two-Photon Microscopy. *J. Am. Chem. Soc.* **2005**, *127*, 11364−11371.
(100) Cichy, B.; Wawrzynczyk, D.; Bednarkiewicz, A.; Samoc, M.; Strek, W. Optical Nonlinearities and Two-Photon Excited Time-Resolved Luminescence in Colloidal Quantum-Confined $CuInS_2$/ZnS Heterostructures. *RSC Adv.* **2014**, *4*, 34065−34072.
(101) Subha, R.; Nalla, V.; Yu, J. H.; Jun, S. W.; Shin, K.; Hyeon, T.; Vijayan, C.; Ji, W. Efficient Photoluminescence of Mn^{2+}-Doped ZnS Quantum Dots Excited by Two-Photon Absorption in near-Infrared Window II. *J. Phys. Chem. C* **2013**, *117*, 20905−20911.
(102) Wang, F.; Deng, R.; Wang, J.; Wang, Q.; Han, Y.; Zhu, H.; Chen, X.; Liu, X. Tuning Upconversion through Energy Migration in Core-Shell Nanoparticles. *Nat. Mater.* **2011**, *10*, 968−973.
(103) Lu, Y.; Zhao, J.; Zhang, R.; Liu, Y.; Liu, D.; Goldys, E. M.; Yang, X.; Xi, P.; Sunna, A.; Lu, J.; Shi, Y.; Leif, R. C.; Huo, Y.; Shen, J.; Piper, J. A.; Robinson, J. P.; Jin, D. Tunable Lifetime Multiplexing Using Luminescent Nanocrystals. *Nat. Photonics* **2014**, *8*, 32−36.
(104) Nam, S. H.; Bae, Y. M.; Park, Y. I.; Kim, J. H.; Kim, H. M.; Choi, J. S.; Lee, K. T.; Hyeon, T.; Suh, Y. D. Long-Term Real-Time Tracking of Lanthanide Ion Doped Upconverting Nanoparticles in Living Cells. *Angew. Chem., Int. Ed.* **2011**, *50*, 6093−6097.
(105) Park, Y. I.; Lee, K. T.; Suh, Y. D.; Hyeon, T. Upconverting Nanoparticles: A Versatile Platform for Wide-Field Two-Photon Microscopy and Multi-Modal *in vivo* Imaging. *Chem. Soc. Rev.* **2015**, *44*, 1302−1317.
(106) Bae, Y. M.; Park, Y. I.; Nam, S. H.; Kim, J. H.; Lee, K.; Kim, H. M.; Yoo, B.; Choi, J. S.; Lee, K. T.; Hyeon, T.; Suh, Y. D. Endocytosis, Intracellular Transport, and Exocytosis of Lanthanide-Doped Upconverting Nanoparticles in Single Living Cells. *Biomaterials* **2012**, *33*, 9080−9086.
(107) Jo, H. L.; Song, Y. H.; Park, J.; Jo, E.-J.; Goh, Y.; Shin, K.; Kim, M.-G.; Lee, K. T. Fast and Background-Free Three-Dimensional (3D) Live-Cell Imaging with Lanthanide-Doped Upconverting Nanoparticles. *Nanoscale* **2015**, *7*, 19397−19402.
(108) Carnall, W. T.; Fields, P. R.; Rajnak, K. Spectral Intensities of the Trivalent Lanthanides and Actinides in Solution. II. Pm^{3+}, Sm^{3+}, Eu^{3+}, Gd^{3+}, Tb^{3+}, Dy^{3+}, and Ho^{3+}. *J. Chem. Phys.* **1968**, *49*, 4412−4423.
(109) Bunzli, J.-C. G.; Piguet, C. Taking Advantage of Luminescent Lanthanide Ions. *Chem. Soc. Rev.* **2005**, *34*, 1048−1077.
(110) Zhang, F.; Shi, Q.; Zhang, Y.; Shi, Y.; Ding, K.; Zhao, D.; Stucky, G. D. Fluorescence Upconversion Microbarcodes for Multiplexed Biological Detection: Nucleic Acid Encoding. *Adv. Mater.* **2011**, *23*, 3775−3779.
(111) Lee, J.; Bisso, P. W.; Srinivas, R. L.; Kim, J. J.; Swiston, A. J.; Doyle, P. S. Universal Process-Inert Encoding Architecture for Polymer Microparticles. *Nat. Mater.* **2014**, *13*, 524−529.
(112) Zheng, X.; Zhu, X.; Lu, Y.; Zhao, J.; Feng, W.; Jia, G.; Wang, F.; Li, F.; Jin, D. High-Contrast Visualization of Upconversion Luminescence in Mice Using Time-Gating Approach. *Anal. Chem.* **2016**, *88*, 3449−3454.
(113) Liu, Q.; Yang, T.; Feng, W.; Li, F. Blue-Emissive Upconversion Nanoparticles for Low-Power-Excited Bioimaging in vivo. *J. Am. Chem. Soc.* **2012**, *134*, 5390−5397.
(114) Liu, Q.; Yin, B.; Yang, T.; Yang, Y.; Shen, Z.; Yao, P.; Li, F. A General Strategy for Biocompatible, High-Effective Upconversion Nanocapsules Based on Triplet-Triplet Annihilation. *J. Am. Chem. Soc.* **2013**, *135*, 5029−5037.
(115) Zou, W.; Visser, C.; Maduro, J. A.; Pshenichnikov, M. S.; Hummelen, J. C. Broadband Dye-Sensitized Upconversion of near-Infrared Light. *Nat. Photonics* **2012**, *6*, 560−564.
(116) Chen, G.; Damasco, J.; Qiu, H.; Shao, W.; Ohulchanskyy, T. Y.; Valiev, R. R.; Wu, X.; Han, G.; Wang, Y.; Yang, C.; Ågren, H.; Prasad, P. N. Energy-Cascaded Upconversion in an Organic Dye-Sensitized Core/Shell Fluoride Nanocrystal. *Nano Lett.* **2015**, *15*, 7400−7407.
(117) Lee, J.; Yoo, B.; Lee, H.; Cha, G. D.; Lee, H.-S.; Cho, Y.; Kim, S. Y.; Seo, H.; Lee, W.; Son, D.; Kang, M.; Kim, H. M.; Park, Y. I.; Hyeon, T.; Kim, D.-H. Ultra-Wideband Multi-Dye-Sensitized Upconverting Nanoparticles for Information Security Application. *Adv. Mater.* **2017**, *29*, 1603169.
(118) Wu, X.; Zhang, Y.; Takle, K.; Bilsel, O.; Li, Z.; Lee, H.; Zhang, Z.; Li, D.; Fan, W.; Duan, C.; Chan, E. M.; Lois, C.; Xiang, Y.; Han, G. Dye-Sensitized Core/Active Shell Upconversion Nanoparticles for Optogenetics and Bioimaging Applications. *ACS Nano* **2016**, *10*, 1060−1066.
(119) Wu, M.; Congreve, D. N.; Wilson, M. W. B.; Jean, J.; Geva, N.; Welborn, M.; Van Voorhis, T.; Bulović, V.; Bawendi, M. G.; Baldo, M. A. Solid-State Infrared-to-Visible Upconversion Sensitized by Colloidal Nanocrystals. *Nat. Photonics* **2016**, *10*, 31−34.
(120) Fischer, S.; Frohlich, B.; Kramer, K. W.; Goldschmidt, J. C. Relation between Excitation Power Density and Er^{3+} Doping Yielding the Highest Absolute Upconversion Quantum Yield. *J. Phys. Chem. C* **2014**, *118*, 30106−30114.
(121) Wang, F.; Liu, X. Upconversion Multicolor Fine-Tuning: Visible to Near-Infrared Emission from Lanthanide-Doped $NaYF_4$ Nanoparticles. *J. Am. Chem. Soc.* **2008**, *130*, 5642−5643.
(122) Tian, G.; Gu, Z.; Zhou, L.; Yin, W.; Liu, X.; Yan, L.; Jin, S.; Ren, W.; Xing, G.; Li, S.; Zhao, Y. Mn^{2+} Dopant-Controlled Synthesis of $NaYF_4$:Yb/Er Upconversion Nanoparticles for *in vivo* Imaging and Drug Delivery. *Adv. Mater.* **2012**, *24*, 1226−1231.
(123) Wu, Z.; Lin, M.; Liang, S.; Liu, Y.; Zhang, H.; Yang, B. Hot-Injection Synthesis of Manganese-Ion-Doped $NaYF_4$:Yb,Er Nanocrystals with Red Up-converting Emission and Tunable Diameter. *Part. Part. Syst. Charact.* **2013**, *30*, 311−315.
(124) Zhan, Q.; Qian, J.; Liang, H.; Somesfalean, G.; Wang, D.; He, S.; Zhang, Z.; Andersson-Engels, S. Using 915 nm Laser Excited Tm^{3+}/Er^{3+}/Ho^{3+}-Doped $NaYbF_4$ Upconversion Nanoparticles for *in vitro* and Deeper *in vivo* Bioimaging without Overheating Irradiation. *ACS Nano* **2011**, *5*, 3744−3757.
(125) Xie, X.; Gao, N.; Deng, R.; Sun, Q.; Xu, Q.-H.; Liu, X. Mechanistic Investigation of Photon Upconversion in Nd^{3+}-Sensitized Core-Shell Nanoparticles. *J. Am. Chem. Soc.* **2013**, *135*, 12608−12611.
(126) Wang, Y.-F.; Liu, G.-Y.; Sun, L.-D.; Xiao, J.-W.; Zhou, J.-C.; Yan, C.-H. Nd^{3+}-Sensitized Upconversion Nanophosphors: Efficient *in vivo* Bioimaging Probes with Minimized Heating Effect. *ACS Nano* **2013**, *7*, 7200−7206.
(127) Shen, J.; Chen, G.; Vu, A.-M.; Fan, W.; Bilsel, O. S.; Chang, C.-C.; Han, G. Engineering the Upconversion Nanoparticle Excitation Wavelength: Cascade Sensitization of Tri-Doped Upconversion Colloidal Nanoparticles at 800 nm. *Adv. Opt. Mater.* **2013**, *1*, 644−650.
(128) Xiong, L.; Yang, T.; Yang, Y.; Xu, C.; Li, F. Long-Term *in vivo* Biodistribution Imaging and Toxicity of Polyacrylic Acid-Coated Upconversion Nanophosphors. *Biomaterials* **2010**, *31*, 7078−7085.
(129) Cheng, L.; Yang, K.; Shao, M.; Lu, X.; Liu, Z. *In Vivo* Pharmacokinetics, Long-Term Biodistribution and Toxicology Study of Functionalized Upconversion Nanoparticles in Mice. *Nanomedicine* **2011**, *6*, 1327−1340.
(130) Park, H. S.; Nam, S. H.; Kim, J.; Shin, H. S.; Suh, Y. D.; Hong, K. S. Clear-Cut Observation of Clearance of Sustainable Upconverting Nanoparticles from Lymphatic System of Small Living Mice. *Sci. Rep.* **2016**, *6*, 27407.

DOI: 10.1021/acscentsci.7b00574
ACS Cent. Sci. 2018, 4, 324−336

(131) Gao, Y.; Zhu, X.; Zhang, Y.; Chen, X.; Wang, L.; Feng, W.; Huang, C.; Li, F. *In vivo* Biodistribution and Passive Accumulation of Upconversion Nanoparticles in Colorectal Cancer Models Via Intraperitoneal Injection. *RSC Adv.* **2017**, *7*, 31588−31596.
(132) Yu, J.; Yin, W.; Peng, T.; Chang, Y. N.; Zu, Y.; Li, J.; He, X.; Ma, X.; Gu, Z.; Zhao, Y. Biodistribution, Excretion, and Toxicity of Polyethyleneimine Modified $NaYF_4$: Yb, Er Upconversion Nanoparticles in Mice Via Different Administration Routes. *Nanoscale* **2017**, *9*, 4497−4507.
(133) Wang, K.; Ma, J.; He, M.; Gao, G.; Xu, H.; Sang, J.; Wang, Y.; Zhao, B.; Cui, D. Toxicity Assessments of near-Infrared Upconversion Luminescent LaF_3:Yb,Er in Early Development of Zebrafish Embryos. *Theranostics* **2013**, *3*, 258−266.
(134) Jayakumar, M. K. G.; Bansal, A.; Li, B. N.; Zhang, Y. Mesoporous Silica-Coated Upconversion Nanocrystals for near Infrared Light-Triggered Control of Gene Expression in Zebrafish. *Nanomedicine* **2015**, *10*, 1051−1061.
(135) Lim, S. F.; Riehn, R.; Ryu, W. S.; Khanarian, N.; Tung, C.-K.; Tank, D.; Austin, R. H. *In vivo* and Scanning Electron Microscopy Imaging of Upconverting Nanophosphors in Caenorhabditis Elegans. *Nano Lett.* **2006**, *6*, 169−174.
(136) Chen, J.; Guo, C.; Wang, M.; Huang, L.; Wang, L.; Mi, C.; Li, J.; Fang, X.; Mao, C.; Xu, S. Controllable Synthesis of $NaYF_4$: Yb,Er Upconversion Nanophosphors and Their Application to in vivo Imaging of Caenorhabditis Elegans. *J. Mater. Chem.* **2011**, *21*, 2632−2638.
(137) Bansal, A.; Liu, H.; Jayakumar, M. K. G.; Andersson-Engels, S.; Zhang, Y. Quasi-Continuous Wave Near-Infrared Excitation of Upconversion Nanoparticles for Optogenetic Manipulation of *C-elegans*. *Small* **2016**, *12*, 1732−1743.
(138) Yang, X.; Stein, E. W.; Ashkenazi, S.; Wang, L. V. Nanoparticles for Photoacoustic Imaging. *WIREs. Nanomed. Nanobiotechnol.* **2009**, *1*, 360−368.
(139) Sun, Y.; Zhu, X.; Peng, J.; Li, F. Core−Shell Lanthanide Upconversion Nanophosphors as Four-Modal Probes for Tumor Angiogenesis Imaging. *ACS Nano* **2013**, *7*, 11290−11300.

DOI: 10.1021/acscentsci.7b00574
ACS Cent. Sci. 2018, 4, 324−336